

# $\lambda/4$ Stepped-Impedance Resonator Bandpass Filters Fabricated on Coplanar Waveguide

Atsushi Sanada, Hiroyuki Takehara, Takashi Yamamoto and Ikuo Awai

Yamaguchi University, Ube, Yamaguchi 755-8611, Japan

**Abstract** — Simple and compact multi-stage microwave bandpass filters (BPFs) using  $\lambda/4$  stepped-impedance resonators (SIRs) fabricated on coplanar waveguide (CPW) are presented, which are applicable for MMICs or High- $T_c$  superconducting filters. An accurate, tuning-free, design method of the  $\lambda/4$  SIR-BPF is demonstrated with assistance of full-wave electromagnetic field simulator, which is based on a conventional filter design method using impedance inverters. Full-wave simulation and experimental results for a two-stage Chebyshev BPF designed at 5GHz agreed well with theoretical results.

## I. INTRODUCTION

A  $\lambda/4$  stepped-impedance resonator (SIR) fabricated on the coplanar waveguide (CPW)[1]-[3] is a resonator which consists of two transmission lines with different characteristic impedances and has advantages in size reduction and good spurious characteristics, and low radiation-Q compared with a uniform transmission line resonator. Having ground planes in the same plane of circuit, the CPW is suitable for a compact  $\lambda/4$  resonator with a short-circuited at one end of the resonator in terms of easy fabrication as well as good adaptability for MMICs. Besides, single side conductor of CPW has reduces total cost of fabrication of the BPF when the high- $T_c$  superconducting (HTS) material is used for the substrate to have a drastic improvement of the conductor-Q of the resonator.

In this paper, a design method of the multi-stage  $\lambda/4$  CPW SIR BPF arranged in-line on a substrate is presented. Since the SIR has two transmission lines with different characteristic impedances with a discontinuity at the conjunction of the two transmission lines, the conventional BPF design theory using a uniform  $\lambda/4$  transmission line resonator cannot be directly applicable. Although, with assistance of a full-wave electromagnetic field simulator, we can describe the SIR with an appropriate equivalent circuit with sufficient accuracy and the sophisticated conventional BPF design method with impedance inverters can be applied to realize tuning-free fabrication.

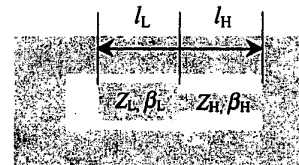
Two- and six-stage Chebyshev SIR BPF designs are demonstrated and equivalent circuit diagrams of the

SIR as well as J- and K-inverters are obtained. Electromagnetic field simulations and experiments for the two-stage SIR BPF are carried out and frequency characteristics of transmission and reflection coefficients are obtained and compared with the theoretical results.

## II. $\lambda/4$ CPW SIR BPF

Figure 1 shows a structure of the  $\lambda/4$  CPW SIR. The CPW SIR consists of two transmission lines with different characteristic impedances. One end of the high impedance line is grounded and the other end of the low impedance line is open-circuited. The size of the SIR can be reduced compared with a uniform  $\lambda/4$  transmission line resonator with the same resonant frequency due to the shunt capacitances at the open end and the series inductance of the short end. The size reduction can be more than about a half of the uniform resonator.

Figure 2 shows typical structures of the  $\lambda/4$  CPW SIR BPFs that are compositions of the SIRs. The  $\lambda/4$  SIRs are arranged facing the open and the short ends of the companions of two neighboring resonators each other as shown in the figure. External input and output circuits can be coupled with the BPF at the both ends of an in-line BPF either capacitively or inductively, or the mixture of those, as shown in Fig.2(a)-(c). All of these can be designed in the same manner that will be discussed in the following section. Regarding coupling circuits in the BPF as impedance inverters, we apply the conventional filter design method for multi-stage BPF[4]. The capacitive coupling circuit and the inductive coupling circuit can be expressed by J- and K-inverter, respectively. Characteristic impedances of the J- and K-inverters can be different from that of the input/output transmission line.



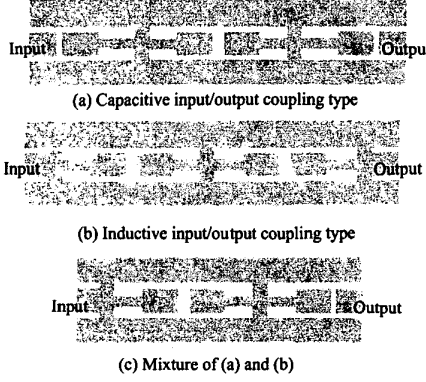


Fig. 2 Examples of  $\lambda/4$  CPW SIR BPFs

### III. DESIGN

In order to demonstrate performance of the  $\lambda/4$  CPW SIR BPF, a two- and six-stage 0.01dB ripple Chebyshev BPF design with center frequency of  $f_0 = 5.000\text{GHz}$  and ripple bandwidth of  $RW = 3.00\%$  is demonstrated. The CPW was designed on a substrate whose thickness  $h = 500\mu\text{m}$  and the relative dielectric constant  $\epsilon_r = 9.6$ . The width of the input/output line is 1.18mm and the distance between the ground planes is 1.82mm, which gives the characteristic impedance of  $50\Omega$ . The circuit pattern and the equivalent circuit of the BPF are shown in Fig.3(a) and (b), respectively.

#### A. CPW SIR

The structural parameters of the  $\lambda/4$  CPW SIR was determined by full-wave electromagnetic field simulations. Let the ratio  $k (=Z_L/Z_H)$  of the two characteristic impedances of the transmission lines in the SIR be 0.5 and the lower characteristic impedance be the same as that of the input/output line of  $50\Omega$ , (i.e.,  $Z_H = 100\Omega$ ), the lengths of the low impedance line ( $l_L$ ) and the high impedance line ( $l_H$ ) are obtained as  $l_L = 2.68\text{mm}$  and  $l_H = 2.72\text{mm}$  from scattering parameters calculated by simulations for the structure shown Fig.1, where  $Z_L$  and  $Z_H$  are the characteristic impedances of the low and high impedance transmission lines of the SIR, respectively. The shunt capacitance  $C_d (=B_d/\omega_0)$  at the discontinuity of the SIR is obtained  $C_d = 0.0195\text{pF}$ , where  $B_d$  is the shunt susceptance due to the capacitance  $C_d$  at the discontinuity and  $\omega_0 = 2\pi f_0$  is a resonant angular frequency.

#### B. Inverters

After modeling the SIR with the equivalent circuit of

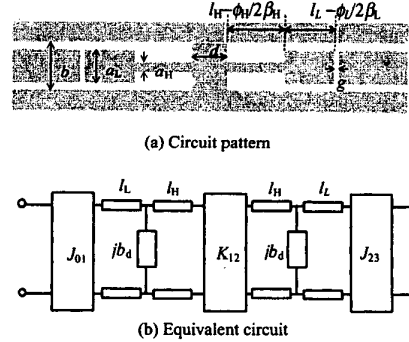


Fig. 3 Two-stage  $\lambda/4$  CPW SIR BPF

two transmission lines and a shunt capacitance, we can theoretically obtain the reactance and susceptance slope parameters looking at the short and open ends of the SIR, respectively, by the circuit theory. Consequently, we can use conventional filter design theory using impedance inverters[4].

The capacitive and reactive coupling are achieved by the J- and K-inverters. The J-inverter can be realized on CPW by either the gap or the interdigital structure as shown Fig.4(a)[4]. The equivalent circuit can be expressed by the  $\Pi$  capacitance network with transmission lines of negative electrical length  $-\phi/2$  at the both sides as shown in Fig.4(b). The circuit parameter can be calculated by scattering parameters obtained by electromagnetic field simulation for the circuit of Fig.4(a). As for the K-inverter shown in Fig.5(a), the T inductance network with transmission lines shown in Fig.5(b) can be used as its equivalent circuit. Scattering parameters obtained by electromagnetic field simulations for the structure of Fig.5(a) in the impedance of  $Z_H (= Z_L/k = 100\Omega)$  system to obtain the circuit parameters of the K-inverter.

#### C. BPF Design

Following the procedure shown in the previous sections, multi-stage SIR BPFs with identical SIRs can be designed. With slope parameters obtained based on the equivalent circuit of the SIR, J- and K-values for the impedance inverters are determined according to the design specifications[4].

The structural parameters of the inverters of Fig.4 and Fig.5 were numerically determined. For two-stage SIR BPF, for example, the equivalent circuit parameters are determined as the capacitance  $C_{se} = 0.0727\text{pF}$ ,  $C_{sh} = 0.0081\text{pF}$ , and electrical length  $\phi = -0.247\text{rad}$ , which

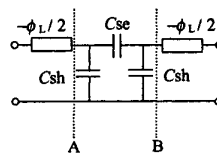
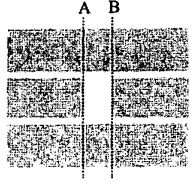
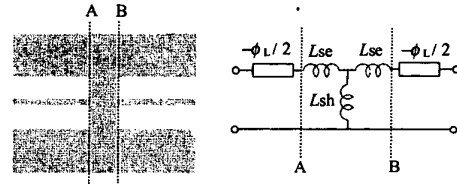


Fig. 4 Capacitive coupling J-inverter



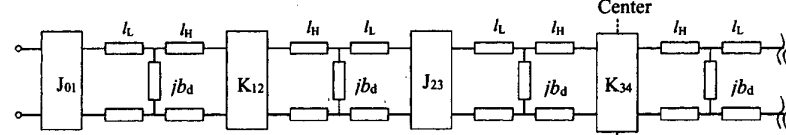
(a) Circuit pattern

(b) Equivalent circuit

Fig. 5 Inductive coupling K-inverter



(a) Circuit pattern



Relative bandwidth of  $w = 0.05$ , ripple  $0.01\text{dB}$ ,  
 $J_{01}/Y_L = 0.1830$ ,  $K_{12}/Z_H = 0.02430$ ,  $J_{23}/Y_L = 0.01727$ ,  $K_{34}/Z_H = 0.01555$ ,  
 $l_L - \phi_{L1}/2\beta_L = 1.696\text{mm}$ ,  $l_L - \phi_{L2}/2\beta_L = 2.301\text{mm}$ ,  $l_H - \phi_{H1}/2\beta_H = 2.563\text{mm}$ ,  $l_H - \phi_{H2}/2\beta_H = 2.568\text{mm}$ ,  
 $l_{ID} = 0.287\text{mm}$ ,  $d_1 = 0.713\text{mm}$ ,  $g_1 = 1.434\text{mm}$ ,  $d_2 = 1.192\text{mm}$ ,  $g_2 = 0.100\text{mm}$

(b) Equivalent circuit

Fig. 6 Six-stage  $\lambda/4$  CPW SIR BPF

correspond to  $J_{01}/Y_L = J_{23}/Y_L = 0.1106$ , where  $Y_L = (1/Z_H = 1/50\text{S})$  is the characteristic admittance of the low impedance transmission line of the SIR. Also,  $L_{sh} = 0.0424\text{nH}$ ,  $L_{se} = 0.1090\text{nH}$ , and  $\phi = -0.0936\text{rad}$  are obtained by the simulation for the K-inverter with  $K_{12}/Z_H = 0.0131$ .

A six-stage BPF designed with  $f_0 = 5.000\text{GHz}$ ,  $BW = 5.00\%$ , and ripple  $0.01\text{dB}$  was also designed by similar procedure to the two-stage BPF design. An interdigital structure is used as input/output J-inverters, since relatively large J value is required. The equivalent circuit of the six-stage BPF with the circuit parameters is shown in Fig.6 (a). The circuit pattern on the CPW structure is shown Fig.6 (b).

#### IV. SIMULATION AND EXPERIMENT

Frequency characteristics of the two- and six-stage BPFs were calculated based on the equivalent circuits shown in Fig.3(b) and Fig.6(b). Passband characteristics

for the BPFs are shown in Fig.7 and 8, respectively, which satisfy the design specification.

Full-wave electromagnetic field simulation was carried out for the two-stage CPW BPF designed in the previous section. The transmission and reflection characteristics were calculated for the circuit pattern with the mesh size of  $20\mu\text{m} \times 20\mu\text{m}$  without tuning the structure. Figure 9 shows  $|S_{21}|$  and  $|S_{11}|$  of the BPF, which agree well with the theory.

Experiments were also carried out. The two-stage BPF fabricated on an MgO substrate ( $t = 0.5\text{mm}$ ,  $\epsilon_r = 9.6$ ,  $\tan\delta = 9 * 10^{-5}$ ) with chemical plating of Cu on a surface with the thickness of  $8\mu\text{m}$ . The frequency characteristics of the BPF are shown in Fig.10, which are also in good agreement with the simulation and validity of the design method is confirmed. It is considered that the deviation of the center frequency between the theoretical and measured results is due to the fabrication error of the circuit pattern and the deviation of the out-of-band characteristic is due to the incomplete package of the BPF.

## V. CONCLUSION

The  $\lambda/4$  CPW SIR BPF structure has been studied and the design method of the BPF with assistance of a full-wave electromagnetic simulator has been shown. Simple two- and six-stage Chebyshev CPW BPF designs have been demonstrated. Frequency characteristics obtained by both the electromagnetic field simulation and the experiment agree well with theoretical results and validity of the design method has been confirmed.

## REFERENCES

- [1] I.Awai, X.Y.Wu, and L.Zhan, "Coplanar stepped-impedance resonator bandpass filter," Proc. of 2000 China-Japan Joint Meeting on Microwaves, pp.1-4, Apr. 2000.
- [2] X.Wu, I.Awai, Z.Yan, K.Wada, and T.Moriyoshi, "Quality Factors of coplanar waveguide resonators," 1999 Asia-Pacific Microwave Conference Proceedings, vol.3, No.3, pp.673-677, Dec. 1999.
- [3] A.Sanada, H.Takehara, T.Yamamoto, and I.Awai, "Design of the CPW in-line  $\lambda/4$  stepped-impedance resonator bandpass filter," 2001 Asia-Pacific Microwave Conference Proceedings, vol.2, pp.633-636, Dec. 2001.
- [4] G.L.Matthaei, et.al., "Microwave Filters, Impedance-Matching Networks, and Coupling Structure," McGraw-Hill, 1964.

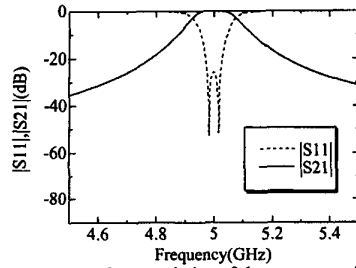


Fig. 7 Frequency characteristics of the two-stage  $\lambda/4$  CPW SIR BPF

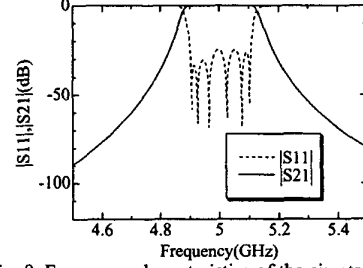
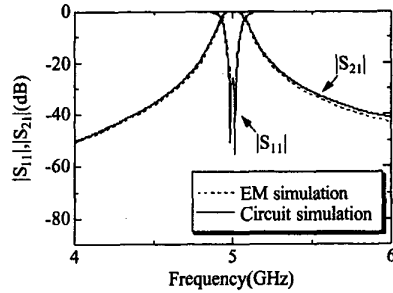
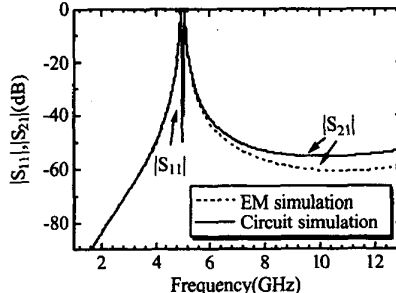


Fig. 8 Frequency characteristics of the six-stage  $\lambda/4$  CPW SIR BPF

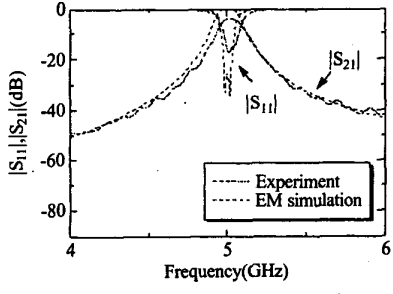


(a) Passband characteristic

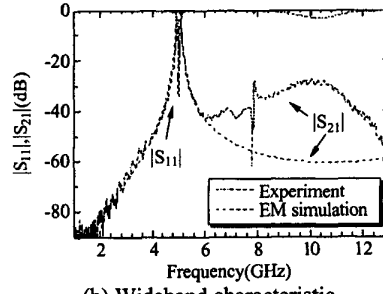


(b) Wideband characteristic

Fig. 9 Full-wave electromagnetic field simulation results



(a) Passband characteristic



(b) Wideband characteristic

Fig. 10 Experimental results